Geophysical Journal International

Geophys. J. Int. (2011) **186,** 6–10 doi: 10.1111/j.1365-246X.2011.05052.x

EXPRESS LETTER

Incorporating metamorphism in geodynamic models: the mass conservation problem

György Hetényi,[1] Vincent Godard,[2] Rodolphe Cattin[3] and James A.D. Connolly[1]

[1] *ETH Zürich, Department of Earth Sciences, Clausiusstrasse 25, 8092 Zürich, Switzerland. E-mail: gyorgy.hetenyi@erdw.ethz.ch*
[2] *CEREGE, Europôle Méditerranéen de l'Arbois, BP80, 13545 Aix-en-Provence Cedex 04, France*
[3] *Géosciences Montpellier, Université Montpellier 2, CC60, Pl. E. Bataillon, 34095 Montpellier Cedex 5, France*

Accepted 2011 April 21. Received 2011 April 21; in original form 2011 March 3

SUMMARY

Geodynamic models incorporating metamorphic phase transformations almost invariably assume the validity of the Boussinesq approximation that violates conservation of mass. In such models metamorphic density changes take place without volumetric effects. We assess the impact of the Boussinesq approximation by comparing models of orogeny accompanied by lower crustal eclogitization both with and without the approximation. Our results demonstrate that the approximation may cause errors approaching 100 per cent in characteristic measures of orogenic shape. Mass conservation errors in Boussinesq models amplify with model time. Mass conservative models of metamorphism are therefore essential to understand long-term tectonic evolution and to assess the importance of the different geodynamic processes.

Key words: Ultra-high pressure metamorphism; Phase transitions; Continental tectonics: compressional; Tectonics and landscape evolution; Dynamics of lithosphere and mantle; Mechanics, theory, and modelling.

1 INTRODUCTION

Geodynamic models of the solid Earth simulate deformation (i.e. collision in the lithosphere and convection in the mantle). They may account for a number of processes that act as the driving forces for deformation, such as convergence and metamorphic phase changes. The models generally solve three constitutive conservation equations: the momentum conservation law, the heat equation and the continuity in mass of the system (e.g. Cserepes *et al*. 1988). Each of these equations can be simplified according to the specific features of the investigated physical problem. In this study we focus on mass conservation, as its simplifications are the most relevant in affecting deformation and in accounting for metamorphism.

The mass-continuity equation requires that any change of mass density ρ in time t must be compensated by a divergence in the flux of mass:

$$\partial\rho/\partial t + \nabla(\rho v) = 0, \tag{1}$$

where v is velocity. Two approximations are commonly applied to this equation. The first is the well-known Boussinesq approximation (Boussinesq 1897), which assumes that density differences are sufficiently small to be neglected, except in the buoyancy term. Therefore density – and hence volume – changes due to deformation are neglected (Figs 1a and b), and eq. (1) is simplified to the incompressible flow formulation:

$$\nabla v = 0. \tag{2}$$

This approximation is made in the overwhelming majority of numerical geodynamic models (e.g. Burov *et al*. 2001 based on Poliakov *et al*. 1993; Kaus *et al*. 2005; Arcay *et al*. 2007; Yamato *et al*. 2007; Braun *et al*. 2008; Rey & Müller 2010). The second approximation concerns the implementation of metamorphism. In simpler cases the inherent variations in density due to varying pressure–temperature (P–T) conditions are not taken into account (Fig. 1a). In more complex models, density changes as a function of P and T, but the induced deformation (volume change) is neglected (Fig. 1b). Physically, the first term $\partial\rho/\partial t$ of eq. (1) is respected, but the second term $\nabla(\rho v) = v\cdot\nabla\rho + \rho\cdot\nabla v$ is simplified to eq. (2) by neglecting the density change driven volumetric variation $v\cdot\nabla\rho$.

There are – to our knowledge – only three modelling tools using the complete form of mass-continuity (Gerya & Yuen 2007; Warren *et al*. 2008 and subsequent works; Afonso & Zlotnik 2011), but differences with respect to previous (incompressible) models are not discussed.

In this paper we advocate for a complete (compressible) solution of the continuity equation that includes the full flow field induced by density changes (Fig. 1c). We argue that the oft-used Boussinesq approximation and metamorphic density changes (exceeding 15 per cent, e.g. Holmes 1965; Liu 1978) have significant

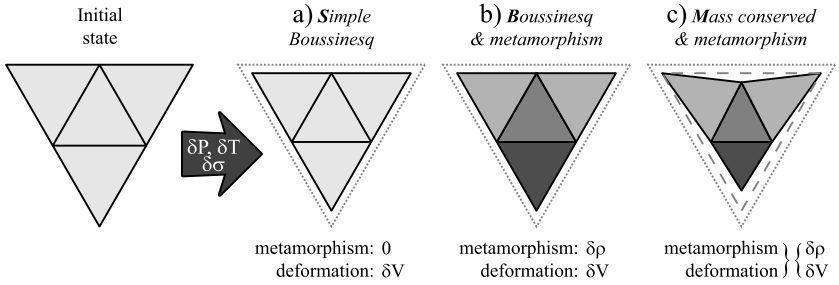

Figure 1. Implementations of metamorphism and deformation into numerical models. Schematic finite elements show changes from the initial state through deformation and varying pressure-temperature conditions (arrow). (a) The simplest models do not account for metamorphism and do not include density variations, even when deformation affects the volume (S model). (b) In the Boussinesq formulation including metamorphism, densities vary as prescribed by phase equilibria calculations, but volume changes are still driven by deformation (B model). Both of the above implementations violate mass-continuity in that volume and density vary independently. (c) Volumetric changes are enforced following density changes according to mass-continuity (M model).

consequences for geodynamic models. Using a simple example, we provide the first direct and quantitative assessment of the continuity-equation formulation's volumetric effects on lithospheric deformation pattern. We focus on this example to draw attention to the potential problems caused by the Boussinesq approximation.

2 METHODS

We focus on the physical effect of the continuity equation formulation and metamorphism by consistently adjusting volume related to mass-continuity when density changes are present (Fig. 1c). Subsequently, we compare the results with those from approximated formulations to assess the consequences on the deformation field.

To account for metamorphic density changes in the *P–T* space we introduce a 'metamorphic' strain tensor that modifies the total strain field of the entire modelled geodynamic system (i.e. applies to all deforming elements, not only those undergoing phase change).

$$\varepsilon^{\text{sys}} = \varepsilon^{\text{sys}} - \varepsilon^{\text{metam}}. \tag{3}$$

Assuming isotropic deformation the metamorphic strain is derived directly from the required density change to respect mass conservation at the element scale:

$$\varepsilon_{ii}^{\text{metam}} = 1/3 \cdot \Delta v/v = -1/3 \cdot \Delta\rho/\rho \ (i = 1, 3), \tag{4}$$

where $\Delta\rho$ is the density change prescribed by phase equilibria calculations. This approach is implemented into a thermo-mechanical finite element modelling tool Cast3M (Verpeaux *et al*. 1988; http://www-cast3m.cea.fr/). This tool features a 2-D geodynamic toolbox that simulates different rheological behaviours, erosion processes and re-meshing. For full details, including resolution scheme, numerical tests, comparisons with other geodynamic modelling tools as well as applications, we refer to Godard *et al*. (2006, 2009) and references therein. An alternative method of accounting for metamorphic density changes would be to express the equation of state as a function of entropy and volume (Connolly 2009). The virtue of this method is that it eliminates singularities in the *P–T* space related to low-order phase transformations. The method is not investigated here because it requires a non-standard numerical formulation, the implementation of which is beyond the scope of this paper.

Our implementation of metamorphic effects follows eqs (3) and (4) with two adaptations for Cast3M: (1) the metamorphic strain is converted to an elastic metamorphic stress because in our implementation stress is the global variable governing the system's deformation; (2) the metamorphic stress is damped to avoid large perturbations in the system – the element's density (volume) will not reach the prescribed value instantaneously, but over a few or few tens of time steps. Because the numerical model involves a large number ($\sim 10^5$–10^6) of time steps we expect and verify that this convergence takes place. Our approach using eq. (3) is straightforward, and does not require major modifications in the numerical resolution scheme of the code. Further details on the implementation are given in Appendix S1 (see Supporting Information).

The three modelling studies mentioned previously that solved the complete form of mass-continuity all used different implementations. Gerya & Yuen (2007) apply a plastic flow rule to express and introduce volumetric changes in terms of dilatant plastic deformation rate. Warren *et al*. (2008) first solve the incompressible formulation (eq. 2) and then add a correcting term in the form of normal forces changing the size of elements, but only during time steps when phase changes take place (therefore this approach does not enforce mass conservation of deforming regions remaining in the same phase). Afonso & Zlotnik (2011) also assume an incompressible media, and apply a local velocity field in the lithosphere that compresses/expands the material undergoing phase change. None of the three models discusses the effect of introducing volumetric changes in their models; therefore a comparison to our procedure and results is infeasible.

3 MODEL SETUP

Our setup simulates intracontinental mountain building following the approach of Avouac & Burov (1996), with, in addition, lower crustal eclogitization. The temporal evolution of a 2-D viscoelastic lithospheric model composed of three layers is analysed, starting with an initial topography and crustal root (Fig. 2). The model imposes horizontal convergence, and accounts for gravitational forces, basal heat flow from the underlying mantle and radiogenic heat production in the crust. The initial temperature field is calculated in steady state at the first time step and is shown in Fig. 2. We simulate surface processes as linear diffusion (e.g. Avouac & Burov 1996), which is a voluntarily simplified but a mass-conserving scheme. Description and quantification of these parameters are shown in Fig. 2 and detailed in Appendix S1.

Metamorphic density changes are anticipated to be the greatest in the lower crust (eclogitization); therefore, for the sake of simplicity and numerical efficiency, we assume constant density for the other layers. In the lower crust, the petrogenetic *P–T–ρ* grid is precalculated using Perple_X (Connolly 2005) using an average lower crustal composition and the procedure proposed in Heténi *et al*. (2007) (see Fig. A2 in Appendix S1). We implement the three formulations of the continuity-equation detailed earlier (Figs 1a–c), and

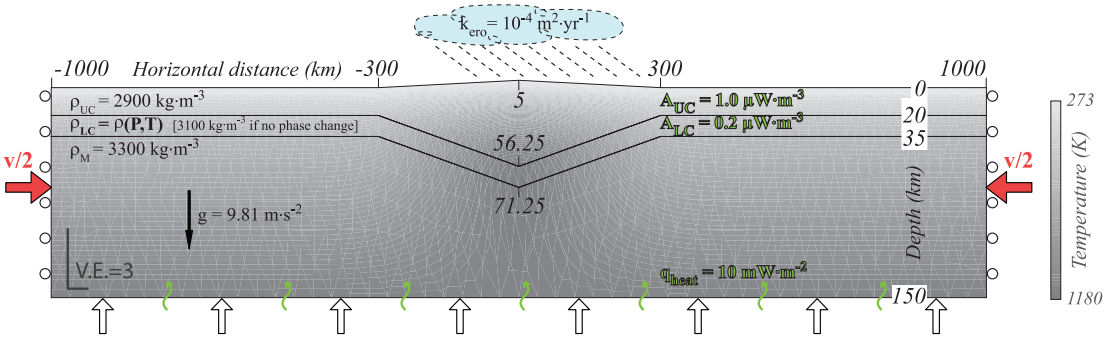

Figure 2. General setup, geometry and the initial temperature field of the model. Modelled geodynamic processes include erosion at surface and metamorphism in the lower crust. These processes as well as boundary conditions are described in the text and in Appendix S1, the resolution of the model is shown in Fig. A1 in Appendix S1.

compare the deformation pattern after a time period of ∼3 Myr. This comparison starts after an initial time of 0.6 Myr during which the main processes (convergence, erosion and metamorphism) are introduced gradually to avoid perturbations at start-up (Appendix S1).

4 RESULTS

We characterize the deformation pattern by focusing on the shape of the topography and of the densifying crustal root. Their evolution in time is visualized through a few characteristic parameters representative of their shape (Fig. 3a). We compare the evolution of these parameters over ∼3 Myr after the initiation time (Figs 3b–g) in the three main models:

(1) the S model with the Boussinesq approximation and without metamorphism (Fig. 1a);
(2) the B model with the Boussinesq approximation and with independent metamorphism (Fig. 1b), which is currently the most widely used type of geodynamic model;
(3) the M model with mass-conservation and with linked metamorphism (Fig. 1c).

The comparison of the deformation patterns' evolution with our simulation settings can be summarized as follows (Figs 3b–g, see density profiles on Fig. A3).

The formulation of metamorphism has no apparent effect on the width of the topography at its base. However, all three models are wider than the initial geometry due to the lateral distribution of material dictated by the diffusive erosion formulation we use.

The mass-conserving formulation creates a similar but slightly (∼3 per cent in 3.2 Myr) higher relief compared with the simple model. Accounting for density variations in the Boussinesq approximated model produces a significantly (∼25 per cent) lower relief and misleadingly suggests greater negative buoyancy associated with metamorphism. This is due to the artificially increased mass of the lower crust as it undergoes eclogitization (higher density, but no decrease of volume). The increasing trend with time is due to continuing horizontal convergence.

The evolution of the foreland basin depth shows large differences: while adding density variations to the S model causes a shallower (∼19 per cent in 3.2 Myr) basin (B model), correcting for the volumetric effects results in a significantly (approximately a factor of 2) deeper basin (M model). The latter effect is related to the more localized downward traction of the densifying crustal root that enhances lateral advection of material from the shoulder area towards the centre of the model. The deeper foreland basin largely contributes to the higher relief (Fig. 3b). In the B model the neglect of the volumetric changes hampers deformation localization and the overall deformation pattern is laterally more distributed.

The base width of the crustal root appears to be controlled by the volumetric effect. When this is correctly implemented, the active orogen has a narrower underlying root due to the increasing density and decreasing volume. The M model's narrowing is greater by 67 per cent relative to the S and B models (with our model settings, at 3.2 Myr). In the incompressible cases (S and B model), in which volume changes are neglected, localization is not enhanced, and this is irrespective of density changes. The general decreasing trend with time is due to the continuing horizontal convergence.

The maximum deepening of the Moho root compared to its initial position shows a faster trend in the case where mass conservation is respected. The B model initially exaggerates the deepening of mass-continuity respecting model due to the artificially increased mass of the crustal root.

The average slope of the crustal root derives from the two previous pictures: a steeper deepening when both mass-continuity and metamorphic density changes are respected. The B model's slope (accidentally) falls near the complete solution by its wider base-width and exaggerated deepening.

Our results suggest that – in addition to convergence, the assumed rheology and surface processes – the implementation of the continuity equation also has important consequences for the evolution and localization of deformation. The principal physical development of the model we propose compared to the previous generations is that it includes both density and strictly bound volume changes that shape the geometry at depth and at surface. In our setup, the density change drives a faster deepening of the lower crustal root relative to models without metamorphism; the volume change avoids the artificial mass generation of the Boussinesq approximation and creates a horizontally narrower, more localized root. Both effects combined make that the horizontal convergence is more efficiently accommodated and converted into vertical mass movement in the orogen, into the deeper root and the higher relief. Hence metamorphic phase changes in combination with the more rigorous implementation of continuity produce a distinctly different deformation pattern and evolution trend than obtained with the various approximations.

To demonstrate the robustness of our approach, the evolution of the total mass of the system with time shows how accurately mass conservation is respected (Fig. 4). While the models lacking a proper implementation of mass-continuity are in constantly increasing error, the model with a consistent implementation continuously respects mass conservation (its deviation from the initial mass is less than the mass of the smallest element, and can be related to numerical noise). At the end of the simulation the total mass in the

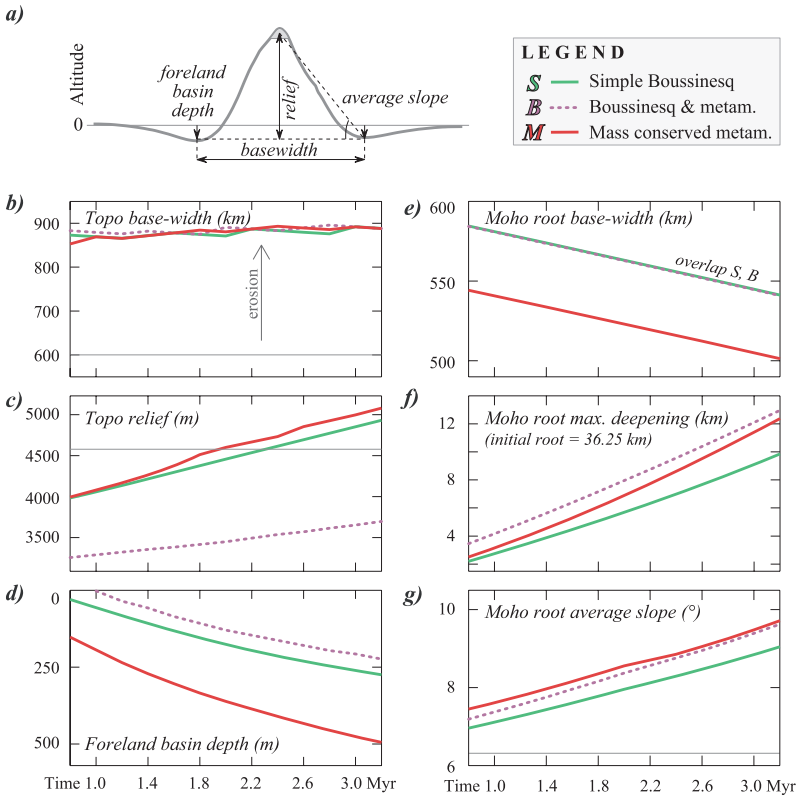

Figure 3. (a) Definition of the parameters describing the shape of the topography high (or, inversely, of the Moho root). The mean altitude of the peak is averaged over 100 km horizontal distance. (b)–(g) Deformation of the model in the three different setups: evolution of the shape parameters describing the geometry of the topography (b–d) and Moho root (e–g). Horizontal thin lines (b, c and g) correspond to the initial level of the values. See text for discussion.

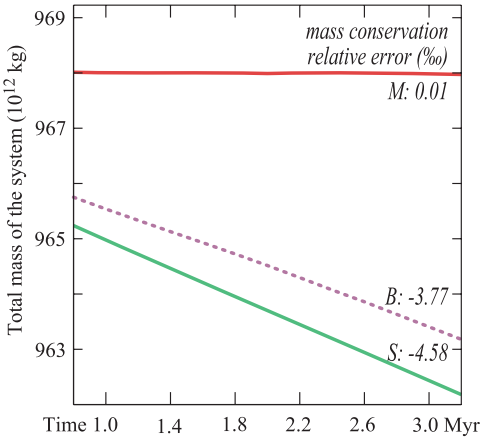

Figure 4. Total mass of the system and the evolution of error for the three models. Relative error is shown at 3.2 Myr. Time is the effective simulation time after the initiation time.

M model records a relative change of 10^{-5}. This is about 2.5 orders of magnitude more accurate than in models with approximated effects of deformation and metamorphism.

5 IMPLICATIONS AND CONCLUSIONS

We showed that the correct implementation of the mass-continuity equation has potentially important consequences on models of lithospheric deformation including metamorphism. To illustrate the effects on the deformation pattern, we built a simple orogenic model, which demonstrates that metamorphism has a key role in shaping the lithospheric structure. Our model also illustrates that the widely used incompressible formulation (Boussinesq approximation) may introduce inaccuracies in mass-continuity and exhibit misleading trends in deformation, in particular when used in conjunction with metamorphic phase changes.

The implications of modelling metamorphism in a physically correct manner are manifold. For instance:

(1) Numerical simulations aiming to reproduce the evolution of exhumation, surface uplift or foreland basin development may be in error when using approximated formulations of mass-continuity. The error is model dependent, but may exceed a factor of 2 for some model parameters as demonstrated by our results on the foreland basin depth. Errors of this magnitude are such that a revision of the previously inferred rates may be necessary to match the same data.

(2) Geologically fast density (and corresponding volume) changes are likely to generate stresses large enough to create fractures or trigger fracturing at depth. The induced stresses can easily exceed the order of a few bars, which is comparable to the stress-drop deduced for earthquakes (Hanks 1977; Scholz 1990). A currently active field example can be the eclogitization of the Indian lower crust beneath Tibet, which spatially coincides with a zone of microseismic activity (Hetényi *et al*. 2007; Whittlinger *et al*. 2009). The accurate resolution of these stresses in geodynamic models requires rigorous solution of the continuity equation.

(3) Metamorphism is shown to influence the shape of the crustal root. In studies where the flexural geometry of a plate is used to estimate lithospheric rheology (e.g. Cattin *et al*. 2001; Hetényi *et al*. 2006; and references therein), a revision of the numerical model may modify the assessed mantle viscosities and lithospheric effective

elastic thickness. The volumetric effects similarly determine the mass distribution and the pressure field within the crustal root and have implications for HP-UHP exhumation processes (e.g. Yamato *et al*. 2007).

(4) If densification and the downward drag of the crustal root are accompanied with rheological softening, the root may become unstable during the long-term evolution of the orogen and enhance decoupling or break-off. The timing of such event will depend on the weight of the crustal root. Incorrect mass estimates resulting from the Boussinesq approximation are likely to lead to false assessment of the timing of decoupling or break-off scenarios and lead to biased conclusions.

Correct modelling of metamorphism that complies with mass conservation is therefore essential to understand long-term tectonic evolution and to assess the respective importance of the different geodynamic processes involved.

ACKNOWLEDGMENTS

We acknowledge the numerous people from ENS Paris and ETH Zurich who provided us with feedback on metamorphism and its effects on geodynamics. In particular we thank Paul Tackley and Taras Gerya for discussion on continuity equation literature, and Alan B. Thompson for his recurrent support and considered opinion. Feedback from attendees at the EGU 2010 conference helped to finalize an earlier draft of the manuscript, which also benefited from the constructive review of J. C. Afonso. We finally thank Philippe Yamato and an anonymous person for their rapid and constructive reviews. This work was supported by the Swiss National Science Foundation grant 200020-107889.

REFERENCES

Afonso, J. C. & Zlotnik, S., 2011. The subductability of the continental lithosphere: the before and after story, in *Frontiers in Earth Sciences, Arc-Continent Collision,* Springer, Berlin, in press.

Arcay, D. *et al.*, 2007. Influence of the precollisional stage on subduction dynamics and the buried crust thermal state: insight from numerical simulations, *Tectonophysics,* **441**, 27–45, doi:10.1016/j.tecto.2007.06.001.

Avouac, J.-P. & Burov, E., 1996. Erosion as a driving mechanism of intracontinental growth, *J. geophys. Res.,* **101**, 17 747–17 769, doi:10.1029/96JB01344.

Boussinesq, M. J., 1897. *Théorie de l'écoulement tourbillonnant et tumultueux des liquides dans les lits rectilignes a grande section,* pp. 1–64, Gauthier-Villars et fils, Paris.

Braun, J. *et al.*, 2008. DOUAR: a new three-dimensional creeping flow numerical model for the solution of geological problems, *Phys. Earth planet. Inter.,* **171**, 76–91, doi:10.1016/j.pepi.2008.05.003.

Burov, E. *et al.*, 2001. A thermomechanical model of exhumation of high pressure (HP) and ultra-high pressure (UHP) metamorphic rocks in Alpine-type collision belts, *Tectonophysics,* **342**, 113–136.

Cattin, R. *et al.*, 2001. Gravity anomalies, crustal structure and thermomechanical support of the Himalaya of Central Nepal, *Geophys. J. Int.,* **147**, 381–392.

Connolly, J. A. D., 2005. Computation of phase equilibria by linear programming: a tool for geodynamic modeling and its application to subduction zone decarbonation, *Earth planet. Sci. Lett.,* **236**, 524–541.

Connolly, J. A.D., 2009. The geodynamic equation of state: what and how, *Geochem. Geophys. Geosyst.,* **10**, Q10014, doi:10.1029/2009GC002540.

Cserepes, L. *et al.*, 1988. Three-dimensional infinite Prandtl number convection in one and two layers with implications for the Earth's gravity field, *J. geophys. Res.,* **93**, 12 009–12 025.

Gerya, T.V. & Yuen, D.A., 2007. Robust characteristics method for modelling multiphase visco-elasto-plastic thermo-mechanical problems, *Phys. Earth planet. Inter.,* **163**, 83–105.

Godard, V. *et al.*, 2006. Numerical modelling of erosion processes in the Himalayas of Nepal: effects of spatial variations of rock strength and precipitation, *Geol. Soc. London Spec. Pub.,* **253**, 341–358.

Godard, V. *et al.*, 2009. Erosional control on the dynamics of low-convergence rate continental plateau margins, *Geophys. J. Int,* **179**, 763–777, doi:10.1111/j.1365-246X.2009.04324.x.

Hanks, T., 1977. Earthquake stress-drops, ambient tectonic stresses, and stresses that drive plates, *Pure appl. Geophys.,* **115**, 441–458.

Hetényi, G. *et al.*, 2006. The effective elastic thickness of the India Plate from receiver function imaging, gravity anomalies and thermomechanical modeling, *Geophys. J. Int.,* **167,** 1106–1118, doi:10.1111/j.1365-246X.2006.03198.x.

Hetényi, G. *et al.*, 2007. Density distribution of the India plate beneath the Tibetan Plateau: geophysical and petrological constraints on the kinetics of lower-crustal eclogitization, *Earth planet. Sci. Lett.,* **264**, 226–244.

Holmes, A., 1965. *Principles of Physical Geology,* 2nd edn, pp. 1–1288, Thomas Nelson and Sons Ltd., London.

Kaus, J.P.B. *et al.*, 2005. Effect of mineral phase transitions on sedimentary basin subsidence and uplift, *Earth planet. Sci. Lett.,* **233**, 213–228.

Liu, L.-G., 1978. High-pressure phase transformations of albite, jadeite and nepheline, *Earth planet. Sci. Lett.,* **37**, 438–444.

Poliakov, A.N.B. *et al.*, 1993. Initiation of salt diapirs with frictional overburden: numerical experiments, *Tectonophysics,* **228**, 199–210.

Rey, P. F. & Müller, R. D., 2010. Fragmentation of active continental plate margins owing to the buoyancy of the mantle wedge, *Nature Geosci.,* **3**, 257–261, doi:10.1038/ngeo825.

Scholz, C., 1990. *The Mechanics of Earthquakes and Faulting,* pp. 1–439, Cambridge University Press, Cambridge.

Verpeaux, P. *et al.*, 1988. Castem2000: une approche moderne du calcul des structures, in *Calcul des Structures et Intelligence Artificielle,* pp. 261–271, eds Fouet, J. M. *et al*., Pluralis, Paris.

Warren, C. J. *et al.*, 2008. Formation and exhumation of ultra-high-pressure rocks during continental collision: role of detachment in the subduction channel, *Geochem. Geophys. Geosyst.,* **9**, Q04019, doi:10.1029/2007GC001839.

Whittlinger, G. *et al.*, 2009. Seismic velocities in Southern Tibet lower crust. A receiver function approach for eclogite detection, *Geophys. J. Int.*, **177**, 1037–1049.

Yamato, P. *et al.*, 2007. Burial and exhumation in a subduction wedge: mutual constraints from thermomechanical modeling and natural P-T-t data (Schistes Lustrés, western Alps), *J. geophys. Res.,* **112**, B07410, doi:10.1029/2006JB004441.

SUPPORTING INFORMATION

Additional Supporting Information may be found in the online version of this article:

Appendix S1. This appendix includes details on: the model setup and input parameters (Section A1); time and timing of processes (A2); the implementation of metamorphism (A3) and numerical limitations (A4) including the corresponding figures.

Please note: Wiley-Blackwell are not responsible for the content or functionality of any supporting materials supplied by the authors. Any queries (other than missing material) should be directed to the corresponding author for the article.

Appendix

This appendix includes details on: the model setup and input parameters (section A.1); time and timing of processes (A.2); the implementation of metamorphism (A.3); numerical limitations (A.4).

A.1. Model setup

The setup of intra-continental mountain building with lower crustal eclogitization is shown in the manuscript (Fig. 2). The model is 2000 km wide and is composed of three layers (20 km thick upper crust, 15 km thick lower crust, 115 km thick mantle). It has an initial topography: a symmetrical, 600 km wide and 5 km high triangle at the centre of the model. The rest of the topography is at sea-level. The size of the crustal root is calculated assuming isostatic thickening of the upper crust. The mesh is composed of linear triangular elements. As our interest is the evolution of topography and deformation of the crustal root, we specify a spatially denser mesh near the surface (see characteristic sizes of elements on Figure A1a).

The rheology of the model is visco-elastic. Elasticity is expressed as a relationship between stress $\boldsymbol{\sigma}$ and strain $\boldsymbol{\varepsilon}$ (e.g., Godard et al., 2009)

$$\varepsilon = \frac{1+\nu}{E} \cdot \sigma - \frac{\nu}{E} \cdot tr\,(\sigma) \cdot 1 \tag{A1}$$

where E is Young's modulus and $\nu = 0.25$ is the Poisson ration. Viscous behavior is described as (e.g., Godard et al., 2009)

$$\dot{\varepsilon} = \gamma_0\,(\Delta\sigma)^n \exp^{(-E_a/RT)} \tag{A2}$$

where $\Delta\boldsymbol{\sigma}$ is the deviatoric stress, R is the universal gas constant, E_a is activation energy, and γ_0 and n are empirically determined constants. The mechanical parameters in equations A1

and A2, together with the thermal parameters of the model including the radiogenic heat production of the layers are summarized in Table A1. The model is submitted to gravitational forces (g = 9.81 m.s^{-2}). The boundary conditions include hydrostatic support from the asthenosphere and free vertical movement on both sides of the model. Horizontal convergence rate of v = 20 mm.yr^{-1} is applied on and equally divided between the two sides of the model. Thermally, a basal heat flow of q_{heat} = 10 mW.m^{-2} is included. Erosion is modeled as a simple linear diffusion (e.g., Avouac & Burov, 1996):

$$\frac{\partial h}{\partial t} = -k_{ero} \cdot \frac{\partial^2 h}{\partial x^2} \quad \text{(A3)}$$

where h is elevation and k_{ero} = 10^{-4} m^2.yr^{-1} is mass diffusivity.

A.2. Time and timing of processes.

All models simulate a total of 4 Myr in time which is sufficiently long to observe the main trends in the deformation pattern. The time step is 20 yr long, resulting in 2.10^5 simulated increments. The mechanical, erosional, thermal and the newly introduced metamorphic strain-(stress-) modification equations are solved in this order at each time step, except for thermal processes (solved at every 100th time step).

To avoid eventual sudden perturbations of the model due to a rapid start-up of geodynamic processes, we use 15% (600 kyr) of the calculation time to gradually increase the power of (Fig. A1b):

(1) convergence, weighed by a factor that increases linearly from 0 to 1 between 4 and 10% of the calculation time (160 and 400 kyr simulated time);

(2) erosion, increasing to full force between 0 and 15 % relative time (600 kyr);

(3) metamorphism, introduced between 10 and 15% (400 and 600 kyr).

The effective simulation of mountain building with all processes present hence starts at 600 kyr (15% calculation time).

For metamorphism, updating the table of prescribed density values based on the current pressure and temperature conditions at each time step is both costly and unnecessary. Considering the rate at which P and T may vary in the model due to convergence and erosion, as well as after testing, we chose to read the density tables every 4 kyr (0.1% relative time).

A.3. Metamorphism

The petrogenetical grids providing density as a function of pressure *P* and temperature *T* are calculated in advance of the thermo-mechanical simulation, to save time and also as the two computational tools operate independently. In our study, we use an average lower crustal composition from Rudnick & Fountain (1995) and Rudnick & Gao (2003) and follow the procedure and selection of solid solutions detailed in Hetényi et al. (2007). We assume water saturated conditions, meaning that all hydrous phases are stabilized in the same proportion. The resulting petrogenetical grid is shown on Figure A2. We note that the pressure used as an input to this grid is calculated as the mean stress rather than mechanical load in order to account for eventual overpressure effects. Finally, as mentioned in the main text, a damping is applied to the stress deriving from metamorphic changes to avoid large perturbations in the system; after testing, we chose to multiply the remaining metamorphic stress by 0.05.

Beyond the curves shown in the manuscript (Fig. 3b-g) which compare the effect of different formulations of metamorphism implemented into numerical models, Figure A3 shows the corresponding density profiles after 3.2 Myr effective simulation time. One can observe (1) the densifying crustal root in M- and B-models, and (2) that the deformation pattern is different when mass-continuity is enforced relative to the incompressible approach (well visible at the crustal root). The slight asymmetries observed in all models are due to the asymmetric initial meshing (Fig. A1), but a higher resolution tests lowering this effect were both computationally expensive and triggered potential instabilities due to the interaction between volumetric effects and re-meshing (see below).

A.4. Numerical limitation

A potential limitation of our approach stems from the presence of two processes that are known to increase the instability of the system. First: global re-meshing of the model may become necessary if the simulated time is long and erosion diminishes the volume of near-surface elements. During re-meshing, the element boundaries are re-drawn and physical fields projected on to the new mesh. The caused perturbation to the system vanishes exponentially over the next time steps. Second: the implemented strain (or stress) enforcing the volumetric changes from metamorphic density variations also perturbs the system. While subsequent events of both re-meshing and density changes occur at some minimum time interval allowing sufficient relaxation time, the numerical solution is potentially divergent when both processes take place nearly simultaneously. The risk of such artifacts can be avoided by (1) adequate choice of the mesh size, (2) delaying one of the processes until the system is relaxed from perturbation related to the other process. In the simulations presented in this paper, no re-meshing was necessary; therefore this type of artifact is not present in our results.

99

100 Reference list

101 Avouac, J.-P. & Burov, E., 1996. Erosion as a driving mechanism of intracontinental growth,
102 *J. Geophys. Res.*, 101, 17,747--17,769, doi:10.1029/96JB01344.
103 Carter, N. L. & Tsenn, M. C., 1987. Flow properties of continental lithosphere,
104 *Tectonophysics,* 136, 27--63.
105 Godard, V., Cattin, R., & Lavé, J., 2009. Erosional control on the dynamics of low-
106 convergence rate continental plateau margins, *Geophys. J. Int*, 179, 763--777,
107 doi:10.1111/j.1365-246X.2009.04324.x
108 Hetényi, G., Cattin, R., Brunet, F., Vergne, J., Bollinger, L., Nábělek, J. L. & Diament, M.,
109 2007. Density distribution of the India plate beneath the Tibetan Plateau: geophysical
110 and petrological constraints on the kinetics of lower-crustal eclogitization, *Earth Planet.*
111 *Sci. Lett.*, 264, 226--244.
112 Kirby, S. H. & Kronenberg, A. K., 1987. Rheology of the lithosphere: Selected topics, *Rev.*
113 *Geophys.,* 25, 1219--1244.
114 Rudnick, R. L. & Fountain, D. M., 1995. Nature and composition of the continental crust – a
115 lower crustal perspective, *Rev. Geophys.*, 33, 267--309.
116 Rudnick, R. L. & Gao, S., 2003. The composition of the continental crust, *in Treatise on*
117 *Geochemistry, Vol. 3: The Crust*, pp. 1--64, ed. Rudnick, R. L., Elsevier-Pergamon,
118 Oxford.
119 Tsenn, M. C. & Carter, N. L., 1987. Upper limits of power law creep of rocks,
120 *Tectonophysics,* 136, 1--26.

121

122

123 Figure legends

Figure A1. (a) Meshing of the numerical simulations and characteristic mesh size at different interfaces in km. (b) Introduction of the different geodynamic processes in time.

Figure A2. Density grid of the lower crust as a function of pressure and temperature. Letters denote the main metamorphic facies: GS – greenschist, BS – blueschist, A – amphibolite, G – granulite, E – eclogite. Bulk composition and selected solid solution are as in the MW model of Hetényi et al. (2007).

Figure A3. Density profile of the three models using different formulations of metamorphism (at 3.2 Myr simulation time).

Tables

	E [GPa]	ρ [kg.m^{-3}]	k W.m^{-1}.K^{-1}]	c [J.kg^{-1}.K^{-1}]	A [μW.m^{-3}]	γ_0 [MPa^{-n}.s^{-1}]	n -	E_a [kJ.mol^{-1}]
Upper crust	20	2900	2.5	1200	1.0	6.03 10^{-24}	2.72	134
Lower crust	20	3100*	2.5	1400	0.2	6.31 10^{-20}	3.05	276
Mantle	70	3300	3.0	1200	0.0	7 10^{-14}	3.0	510

Table A1. Parameter values of the thermo-mechanical model: Young's modulus E, density ρ, thermal conductivity k, specific heat capacity c, radiogenic heat production A, empirically determined parameters to describe viscous behavior γ_0 and n, and activation energy E_a. The star at the lower crustal density denotes that this value is only an initial condition and is dependent on P-T conditions all along the calculation (except for the simple S-model). Parameter values after Carter & Tsenn (1987), Kirby & Kronenberg (1987) and Tsenn & Carter (1987).

a) Caracteristic meshing size of the reference model (km)

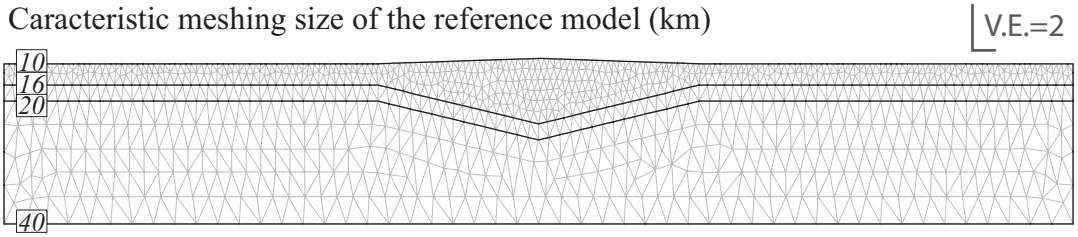

b) Introduction of different processes

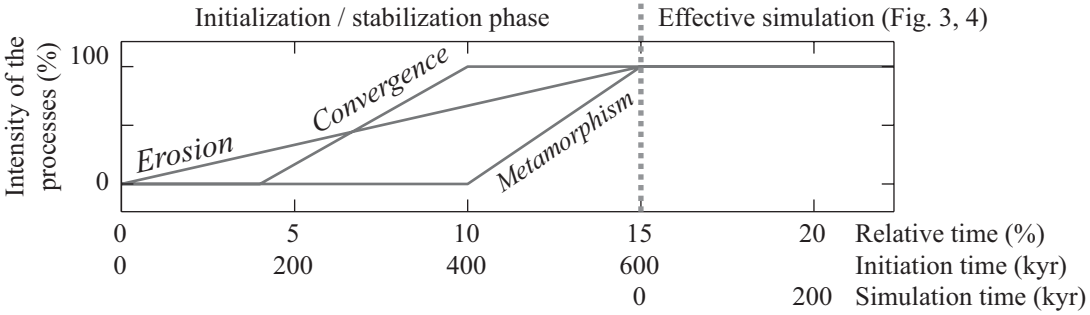

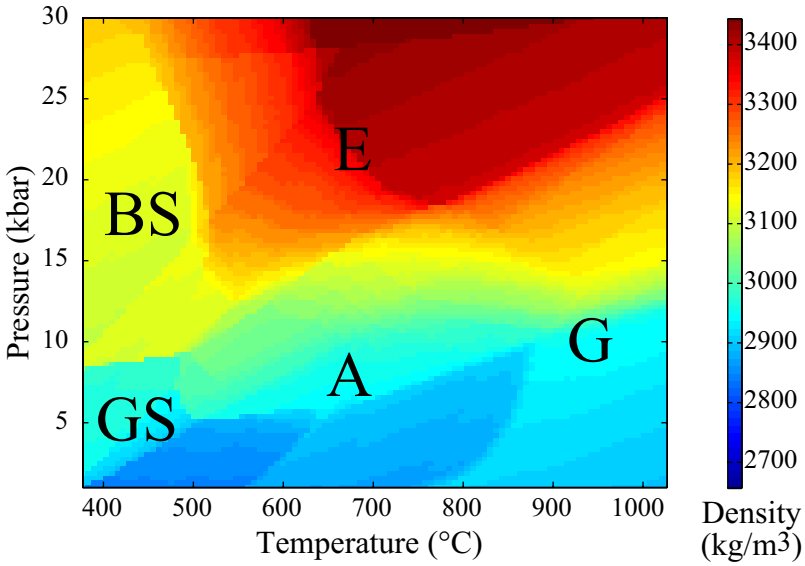
30
25
20
15
10
5
Pressure (kbar)
400
500
600
700
800
900
1000
Temperature (°C)
E
BS
G
A
GS
3400
3300
3200
3100
3000
2900
2800
2700
Density
(kg/m3)

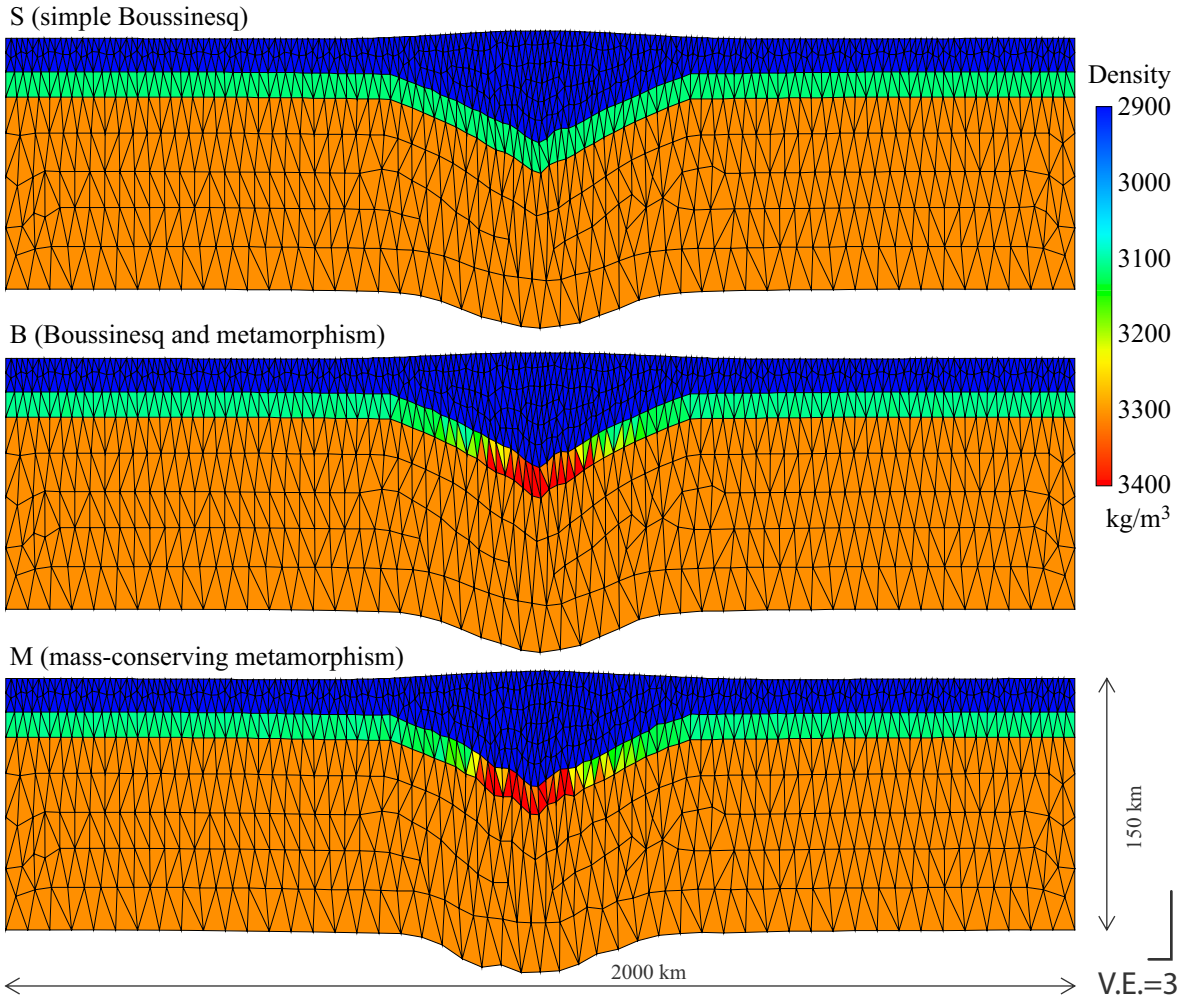
S (simple Boussinesq)
B (Boussinesq and metamorphism)
M (mass-conserving metamorphism)
Density
2900
3000
3100
3200
3300
3400
kg/m3
150 km
2000 km
V.E.=3